Feasibility study for *ex vivo* fluorescence confocal microscopy (FCM) on diagnostic prostate biopsies

Ulf Titze[1]^, Torsten Hansen[1]^, Barbara Titze[1], Birte Schulz[1], Alfons Gunnemann[2]^, Bernardo Rocco[3]^, Karl-Dietrich Sievert[2]^

[1]Department of Pathology, Klinikum Lippe GmbH, Detmold, Germany; [2]Department of Urology, Klinikum Lippe GmbH, Detmold, Germany; [3]Department of Urology, University of Modena and Reggio Emilia, Modena, Italy

Correspondence to: Dr. med. Ulf Titze. Department of Pathology, Klinikum Lippe GmbH, Röntgenstraße 18, 32756 Detmold, Germany. Email: ulf.titze@klinikum-lippe.de.

Background: Fluorescence confocal microscopy (FCM) is a novel micro-imaging technique providing optical sections of examined tissue. The method has been well established for the diagnosis of tumours in dermatological specimens. Preliminary results found good feasibility when this technique was used to examine prostate cancer (PCa) specimens.

Methods: We report on the application of FCM in magnet resonance imaging (MRI)-fused prostate biopsies (10 patients, total number of biopsy specimens: n=121) and compare the results to conventional histology.

Results: Specific structures of the prostatic tissue were very well represented in the FCM images comparable to conventional histology. Prostate carcinoma was diagnosed with good sensitivity (79/68%) and high specificity (100%) by two pathologists with substantial/almost perfect levels of agreement with the results of conventional histology (kappa 0.79/0.86). Depending on the quality of the scans, malignant lesions of 1.8 mm and more in diameter were reliably diagnosed. Smaller lesions were rated as suspect for malignancy, but could not be consistently differentiated from reactive changes. Optimal image qualities were achieved in focus depths of up to 50 μm, whereas deeper scans led to insufficient representation of cytological features. Pre-treatment with acridine orange (AO) did not alter immunoreactivity of the tissue or its feasibility for fluorescence in situ hybridization (FISH) analyses and adequate amounts of DNA could be extracted for further polymerase chain reaction (PCR)-based examinations.

Conclusions: FCM seems to be a promising tool for the timely diagnosis in cases of PCa in patients requiring therapy. In particular, this technique is a material-sparing method that conserves the biopsies as unfixed material for further analysis such as molecular tumour companion diagnosis.

Keywords: Confocal microscopy; prostate cancer (PCa); prostate biopsies; digital pathology

^ ORCID: Ulf Titze, 0000-0002-3791-8929; Torsten Hansen, 0000-0001-7885-0580; Alfons Gunnemann, 0000-0002-0793-5111; Bernardo Rocco, 0000-0003-2946-7424; Karl-Dietrich Sievert, 0000-0003-4814-214x.

Introduction

Prostate cancer (PCa)

PCa is the second most common cancer in men. An estimated 1.1 million cases were diagnosed worldwide in 2012, accounting for 15% of in men diagnosed cancers. PCa incidence varies more than 25-fold worldwide; the rates are highest in Australia/New Zealand, Northern America and in Western and Northern Europe, largely because the widespread practice of prostate specific antigen (PSA) testing and subsequent biopsy in those regions. Autopsy studies reported a prevalence of PCa of 5% by age <30 years increasing to a prevalence of 59% (48–71%) by age >79 years. The age-standardized incidence of PCa varies worldwide. The highest incidence worldwide is found in the USA (124.8/100,000), especially among African-American men (185.4/100,000). PCa is the fifth leading cause of death from cancer in men, with an estimated 307,000 deaths representing 6.6% of the total male cancer mortality. There is relatively less variation in mortality rates worldwide with the number of deaths from PCa larger in less than developed regions (1).

The clinical diagnosis of PCa by the urologist is currently based on the patient's medical history, rectal digital rectal exam and serum PSA. The diagnosis of clinical suspicion of PCa is verified histologically in trans-rectal or trans-perineal biopsies. The histological diagnosis of PCa is based on a combination of histo-architectonic and cytological features (2). In difficult cases, conventional histology can be supplemented using further immunohistochemical techniques. In addition to the proof of malignancy, the pathologist reports on the number of involved biopsies and the degrees of infiltration. Furthermore, the tumour infiltrates are assigned to Gleason scores, based on the histological growth pattern (3,4). Additional imaging is also used to differentiate between localized disease (cT1–2, N0, M0), locally advanced disease (cT3–4, N0, M0) or metastatic stages (any T, cN1, cM1). The risk stratification of locally limited PCa is based on serum PSA and Gleason score (5).

In recent years, remarkable progress has been made in discovering molecular mechanisms of PCa that have led to the development of a variety of diagnostic and prognostic assays on serum, urine and tumour-tissue (6). While these tests open up new possibilities for diagnostics, prognosis and therapy decisions, challenges arise with regard to their integration into patient management (7).

Fluorescence confocal microscopy (FCM)

FCM is an imaging technique that provides optical sections of the examined tissue in a focal plane that can be selected within technical limits (8). It is already established in routine diagnosis of neoplastic and inflammatory skin diseases. Dermatoscopic devices using reflected laser light only allow non-invasive *in vivo* examination of skin lesions [reflected confocal microscopy (RCM)] (9). For the *ex-vivo* examination of surgical skin specimens, confocal microscopes are available which, in addition to reflected laser light, also use fluorescence light (FCM) and require pre-treatment of the tissue with fluorescent dyes (10).

FCM allows timely histological diagnoses from surgical specimens, similar to frozen sections, without any loss of tissue. Initial publications of other organ tumours with FCM reported promising results (11). Recent reports showed that FCM is well suited for intraoperative examination of prostate tissue using post-op biopsy cylinders taken from unfixed prostatectomy specimens (12,13).

We present our first experiences in the evaluation of prostate biopsies by means of FCM. The primary endpoint of our investigations was the level of agreement between diagnoses based on FCM in the operating room and subsequent conventional histology. The secondary goal was to evaluate the suitability of tissue pre-treated for FCM for future molecular examinations based on fluorescence in situ hybridization (FISH) or polymerase chain reaction (PCR).

Methods

Study participants

Prostate biopsies of 10 patients from the Department of Urology of the Hospital (mean age 65.5±10.0, range 49–79 years) were examined. Three patients were under active surveillance (AS) of previously diagnosed PCa, while the other seven patients had clinical suspicion of PCa. Current magnet resonance imaging (MRI) of the prostate was available from eight of the patients. Before the biopsies were taken, the study participants were informed and all signed a written consent. The study was approved by the local Ethical Committee and carried out according to the ethical principles of the Helsinki Declaration (2013).

Confocal microscope

The confocal microscope used in this study was a VivaScope®

2500 M-G4 laser scanning microscope from MAVIG, Munich, Germany. The microscope is equipped with a water immersion objective with 38x magnification and a numerical aperture of 0.85. Illumination of the specimen is performed using two lasers with wavelengths of 488 nm (ultraviolet) and 785 nm (infrared). The short-wave laser demonstrates the cell nuclei marked with fluorescent dye before the examination. The cytoplasmic and extracellular structures, on the other hand, are represented by the reflected light of the long-wave laser. A built-in algorithm transforms the recorded grey values into an image similar to haematoxylin-eosin (H&E) staining, in which the nuclei are shown in violet whereas cytoplasm and extracellular structures are transformed in pink (14). Balance of the staining intensity of nuclear and cellular/extracellular structures is modified by the intensity of the illuminating lasers. The system achieves a total magnification of 550×. According to the manufacturer, tissue samples up to 2.5×2.5 cm in size can be examined (15).

Study design

MRI-fused biopsies (targeted from suspicious lesions in MRI and systematic) were obtained from each patient and examined with FCM and in conventional histology subsequently. The FCM scans were immediately examined by an experienced uro-pathologist (UT) in the operating room during the biopsy procedure. Regardless of the FCM diagnoses, conventional histological sections of the formalin fixed paraffine embedded (FFPE) biopsies were blindly diagnosed by a second pathologist (TH) with experience in urologic pathology. After conventional histological examinations were completed, FCM-scans were re-examined blindly by a third pathologist (BT) as well as the FFPE material was blindly re-examined by a fourth pathologist (BS).

Image-acquisition and sample processing

The native biopsy cylinders were placed on tissue foam pads and instantly pre-treated with pure alcohol for 10 seconds (protein precipitation to enhance contrast). The tissue was then incubated for 30 seconds with an acridine orange solution (AO, 0.6 mM; Sigma-Aldrich®). AO is an intercalating fluorochrome for staining nucleic acids, whose DNA-dye complexes have an extinction maximum (Ex) of 502 nm and an emission maximum (Em) of 526 nm (16).

The tissue samples on the foam pads were placed between two specimen slides specially modified with magnets to standardize the required distance and hold the foam and the tissue in place using continuous pressure. After positioning into the specimen holder of the microscope the scanning process started immediately.

The microscope was controlled using a high-power personal computer. The software delivered a life-view of a small sector of the image obtained. In life-view mode, focus-depth and intensity of the illuminating lasers were adjusted. The user had the choice between the original grayscales and the pseudo-coloured images in life view. After the adjustments were defined, the whole specimen was systematically scanned within 2–3 minutes. The resulting image-scan was issued on the high definition LCD-display, immediately diagnosed by the pathologist (UT) and demonstrated to the urologist.

After the scanning process, the tissue was immediately placed in the intended embedding capsules and fixed in 4% PBS-buffered formaldehyde for 24 h. Further histological processing was carried out for all biopsy cylinders following the standard procedure for FFPE tissue. In order to optimally compare the digital scan and the histological section, the tissue cylinders were processed together with the foam pads.

Histological evaluation and statistical analysis

The FCM-scans were assessed in regard to scan quality (good/bad). Furthermore, the presence of prostate parenchyma and periprostatic tissue (muscles, nerves, adipose tissue, vessels), evidence of tumour manifestations and presence of atypical glands not diagnostic for PCa were documented using a binary variable system (0/1). In case of tumour involvement, Gleason/ISUP-grade and degree of infiltration (%) were documented.

The histological slides were blindly assessed the next day by a second uro-pathologist (TH) in order to avoid any delay in patient management. If necessary, additional immunohistological staining for p40 and AMACR (both polyclonal antibodies, ZytomedSystems, Berlin, Germany) was carried out using the Ventana Benchmark™ (Ventana Medical Systems, Tucson, AZ, USA) immunostainer platform. In accordance with the applicable diagnostic guidelines, tumour manifestations, expansion, Gleason score, perineural or lymphovascular infiltrates and an extraprostatic manifestation were documented for each biopsy in a similar binary variable system.

Statistical analysis was performed using Microsoft Excel™. The consistency of the diagnoses based on the

Table 1 Clinical data, number of biopsies and histological diagnoses in FFPE-material

Patient	Clinical data				FFPE (TH)		FFPE (BS)	
	Age	Indication	PIRADS	Biopsies	PCa	ISUP	PCa	ISUP
P01	65	AS	4	12	6	1	6	1
P02	68	Pre	4	17	0	–	0	–
P03	77	AS	3	10	2	3	2	2
P04	66	Pre	5	10	0	–	0	–
P05	79	Pre	5	12	1	1	1	1
P06	60	AS	–	12	0	–	0	–
P07	57	Pre	5	12	5	2	5	2
P08	49	Pre	5	12	0	–	0	–
P09	57	Pre	2	12	5	3	5	3
P10	77	Pre	–	12	0	–	0	–
Max	79			17	6	3	6	3
Min	49			10	1	1	0	1
Mean	65.5			12.1	1.9		1.9	
SD	10.0			1.9	2.5		2.5	

Clinical data included age, biopsy indication (AS: follow-up in active surveillance *vs*. Pre: pre-therapeutic biopsy because of clinical suspicion on malignancy), PIRADS score and the number of biopsies investigated both in FCM and conventional histology. Histological diagnoses show the number of biopsies involved by tumour (PCa) and ISUP-grading. FFPE, formalin fixed paraffine embedded; PCa, prostate cancer; FCM, fluorescence confocal microscopy.

FCM images with the conventional histology for the individual findings was analysed in an error matrix. The levels of observer agreement was measured using the Cohen's kappa (17) and interpreted according to the categories according to Landis and Koch (18).

Suitability of the material for subsequent examinations

After completing FFPE procedure, residual material of two tumour-infiltrated punch cylinders was examined in FISH against HER2 and Chromosom17-Centromer (ZytoLight FISH-Tissue Implementation Kit, ZytoLight SPEC ERBB2/CEN 17 Dual Color Probe). The *HER2* gene was labelled with ZyGreen (Em: 503 nm, Ex: 528 nm, equivalent to FITC), the *CEP17* gene was marked with ZyOrange (Ex: 547 nm, Em: 572 nm, equivalent to Rhodanine). DAPI (Ex: 358 nm, Em: 461 nm) was used for nuclear staining.

Since AO (Ex: 502 nm, Em: 526 nm) has similar absorption and emission spectra like ZyGreen/FITC (Ex: 503 nm, Em: 528 nm), pre-treatment for FCM might interfere with conventional FISH by outshining its delicate

signals. Further FISH investigations must therefore be performed in deeper tissue regions of the biopsy cylinder, that were not dyed by AO. We measured the maximum penetration depth of AO using native prostate parenchyma taken from another case of prostatectomy examined in frozen section treated for 30 s accordingly. The microscopic investigations were performed using a BX-43 epi-fluorescence microscope (Olympus, Tokio).

In addition, DNA was extracted from two comparable tumour-free biopsies from four patients, one of each had been pre-treated for FCM, whereas the counterpart had been exclusively FFPE-processed. DNA-concentration was determined by photometry as previously described (19) and then analysed statistically by Student *t*-test for dependent variables.

Results

Clinical data, number of biopsies examined with FCM and histological diagnoses based on the FFPE material are shown in *Table 1*. Both FCM scans and conventional
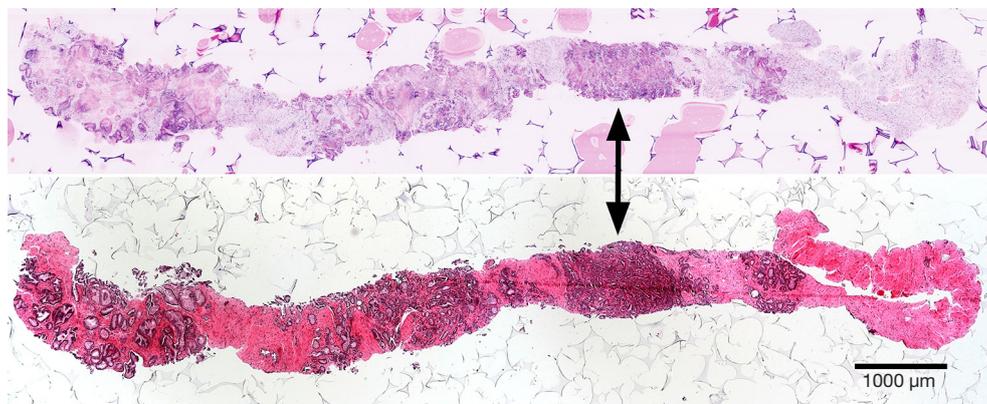
1326

Titze et al. Feasibility of FCM in the assessment of prostate biopsies

Figure 1 Comparison of FCM-scan and conventional H&E-morphology. FCM scan (top) of a biopsy (P01–09) shows a matching representation of tissue structures with the H&E-stain of FFPE-processed material (bottom). Areas of stroma and glands can be unequivocally correlated. Regularly shaped pre-existing glands and hyper-cellular fields with malignant micro-acinar proliferations (arrow) are easily distinguished at low magnification. FCM, fluorescence confocal microscopy; H&E, haematoxylin-eosin; FFPE, formalin fixed paraffine embedded.

histological slides were available from 121 biopsy cylinders. 3/10 patients were under AS of previously diagnosed PCa, 7/10 patients were in pre-therapeutic setting (Pre) with clinical suspicion of malignancy. In conventional histology, tumour involvement was consistently diagnosed in 5/10 patients (P01, P03, P05, P07 and P09, 19/121 biopsy cylinders, 15.7%) blindly by two pathologists (TH, BS). The sizes of tumour lesions ranged between 0.5 and 10 mm (mean value 3.7±3.1 mm). Two cases showed Gleason pattern 3+3, in three cases Gleason 4 patterns were present. Two of these cases were consistently graded as Gleason 3+4 (ISUP2) and Gleason 4+3 (ISUP3) in blinded re-evaluation of the histological slides. One case resulted in a different ISUP graduations (ISUP2 *vs*. ISUP 3).

Pre-treatment of the biopsies for FCM took between 1 and 2 minutes. The scanning process took 2–3 minutes, so that an entire time of approximately 5 minutes could be assumed for each biopsy. The FCM scan was then assessed on the computer subsequently in the operating room. Additional biopsies were stored on the foam pads and impregnated with NaCl for several minutes without any loss of quality. Therefore, no delays in the duration of the biopsy procedure or anaesthesia resulted due to the FCM examinations.

The representation of the tissue in the FCM scans seemed very similar to that of frozen sections. Architectural features of the tissues were very well reproduced (*Figure 1*), thereby enabling a direct correlation of the FCM images and conventional sections. Stroma-rich regions as well as

smaller glandular structures could be unequivocally assigned in the paraffin sections. Extra-prostatic tissues (fat, muscles, nerves, vessels) were unmistakably identified. Due to the lack of fixation of the material, cytological features were only partially comparable to the gold standard of FFPE-processing. In tumour cells, nuclear hyperchromasy and enlarged nuclei were not reproduced as reliably as after FFPE-processing.

For optimal FCM image quality, it was important to find the correct focus depth and the optimal balance of reflection and fluorescence intensity. The best scanning qualities were achieved with focus depths between 20 and 50 µm. Deeper scans resulted in inhomogeneous fluorescence signals (*Figure 2*) making the assessment of nuclear features even more difficult or impossible. This effect was due to a reduced uptake of fluorochrome in deeper tissue. In material of a frozen section examination that were stained with AO for 30 seconds, we measured a penetration depth of up to 100 µm in maximum (*Figure 3*) while deeper tissue portions were not dyed by the fluorochrome.

The FCM diagnoses are shown in *Table 2*. Intraoperatively, the pathologist UT correctly assessed 15 of the 19 tumour manifestations (4× false negative, 0× false positive, sensitivity 79%, specificity 100%). Pathologist BT diagnosed 13 tumour manifestations correctly (6× false negative, 0× false positive, sensitivity 68%, specificity 100%). Statistical analyses showed substantial (kappa 0.79, BT) respectively almost perfect (kappa 0.86, UT) levels of agreement with the FFPE-diagnoses according to the
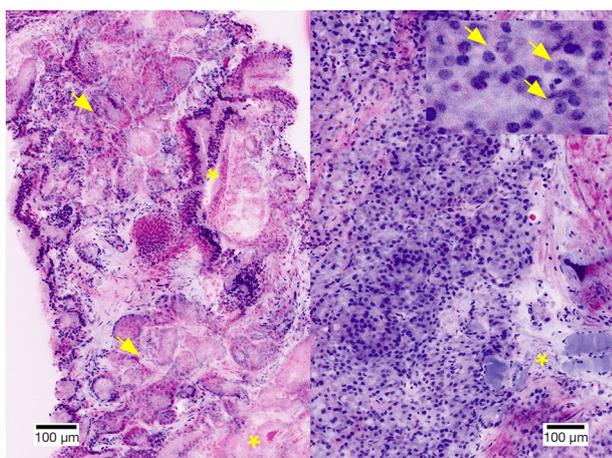
Figure 2 Image quality depending on the depth of focus. Left side: FCM-scan of a biopsy (P01–09) showing Gleason 3 tumour (arrows) and pre-existing glands (*). This example shows effects of a scan in too deep tissue with pale nuclei in the middle of the picture whereas nuclei are clearly depicted in the periphery. Right side: FCM-scan of a biopsy (P09–08) showing Gleason 4 pattern with extra-prostatic growth between skeletal muscle (*). This example is an optimal result showing homogeneous signals of the nuclei that are clearly depicted. At higher magnification (inlay), cytological features like enlarged nucleoli (arrows) can easily be identified. FCM, fluorescence confocal microscopy.
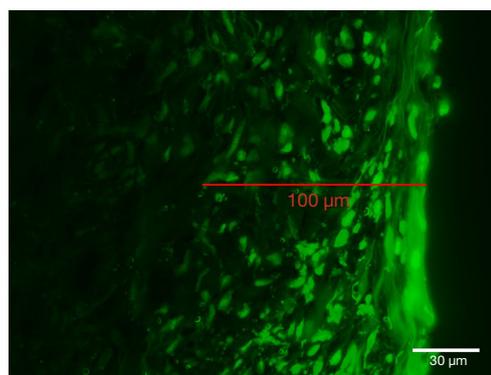

Figure 3 Measurement of penetration depth of AO in frozen section material. Fluorescence microscopy of a frozen section taken from a prostatectomy-specimen shows nuclear labelling of cells in up to 100 μm. Nuclei in deeper regions of the tissue are not stained with AO. AO, acridine orange.

categories of Landis and Koch (18). One case of high-grade tumour (P07) was incorrectly diagnosed ISUP grade 1 intraoperatively (UT), but not in the post-hoc evaluation (BT).

Table 3 summarizes the tumour-infiltrated biopsies, showing size and Gleason-pattern of the tumour-infiltrates based on the FFPE-diagnoses as well as the FCM-diagnoses (presence of carcinoma and/or atypical glands). In some biopsies in the first patient (P01–02, P01–03, P01–12), small infiltrates of well differentiated acinar carcinoma with sizes between 0.5 and 1 mm had been obtained, which were found not diagnostic for PCa by either pathologist (UT and BT) in the FCM, but were documented as atypical glands only. Larger tumour manifestations (P01–06, P01–08, P01–09) ranging from 1.8 to 8 mm in diameter were consistently diagnosed as malignant by both pathologists. In biopsy P05–07, infiltrates of a well differentiated carcinoma with 4 mm size were present, which were difficult to characterize by the less experienced pathologist (BT) because of reduced usability of cytological features. False negative diagnoses of biopsies P07–02 and P07–12 were due to insufficient quality

of the FCM-scans caused by suboptimal focus planes.

The small tumour lesions could only be classified as malignant in the paraffin material using additional immunohistology. The immune reactions for p40 and AMACR were carried out without restriction on the material pre-treated for FCM (*Figure 4*). There was no difference in staining compared to the material that was exclusively FFPE-processed. Thus, treatment with alcohol and AO is not expected to limit immunoreactivity of the tissue.

Our FISH analysis for HER2 and CEP17 on those biopsies pre-treated for FCM showed flawless labelling of cell nuclei with DAPI (*Figure 5*). In situ hybridizations for the HER2 and CEP17 probes demonstrated excellent results with clearly separated signals. Although ZyGreen/FITC and AO have similar absorption and emission spectra, the FISH signal was not disturbed by the previously applied pre-treatment.

There were no significant differences in the amount of DNA from FFPE-processed biopsies compared to the material pre-screened with FCM (0.17 ± 0.04 *vs.* 0.23 ± 0.1 ng/μL, P=0.254).

Discussion

In recent years, several microscopic methods have been developed for *ex vivo* examinations of unfixed tissue based on modifications of illumination, fluorescence techniques and digital image processing. Although these methods are mainly used in neurosciences and developmental biology,

Table 2 Comparison of histological diagnoses in FFPE-sections and FCM-scans

Patient	Biopsies	FFPE diagnosis (HA, BS)			FCM (UT)		FCM (BT)	
		Benign	PCa	ISUP	PCa	ISUP	PCa	ISUP
P01	12	6	6	1	3	1	3	1
P02	17	17	0	–	0	–	0	–
P03	10	8	2	3/2	2	2	2	2
P04	10	10	0	–	0	–	0	–
P05	12	11	1	1	1	1	1	1
P06	12	12	0	–	0	–	0	–
P07	12	7	5	2	4	1	2	2
P08	12	12	0	–	0	–	0	–
P09	12	7	5	3	5	3	5	4
P10	12	12	0	–	0	–	0	–
Total	121	102	19		15		13	
False-negative tumour diagnoses					4		6	
False-positive tumour diagnoses					0		0	
Sensitivity					79%		68%	
Specificity					100%		100%	
Cohens Kappa					0.86		0.79	
Level of agreement (Landis & Koch)					Almost perfect		Substantial	
Wrong ISUP <2						1		0

For each patient, number of benign and tumour-involved biopsies as well as ISUP grades are shown in conventional histology (FFPE) compared to the diagnoses in FCM. FFPE, formalin fixed paraffine embedded; FCM, fluorescence confocal microscopy; PCa, prostate cancer.

promising results have been published for the investigation of prostate tissue (20-22). FCM is a technique based on a combination of confocal imaging and fluorescence microscopy enabling *ex-vivo* examination of fresh tissues with focus depths up to 100 μm.

The device used in this study provided fast images of the fresh tissue feasible for diagnosis under anaesthesia. The optimal image quality was achieved by practice. Representation of cytological features strongly depended on the optimal focus levels and sometimes was very variable even within a single image. In our experiences, this turned out to be a disadvantage for the diagnosis of smaller lesions. Very good representation of histoarchitectural finding were sufficient for the diagnosis of larger tumour lesions and detection of higher Gleason grades. Therefore, in spite of some limitations in the representation of cytologic features, this technique is a promising tool for the timely detection of

PCa in the operating room. In our first 10 patients, tumour manifestations of 1.8 mm or more were reliably diagnosed and assigned to Gleason patterns in the FCM.

Smaller lesions of well differentiated tumour were only found suspicious for malignancy or misdiagnosed as reactive changes in FCM. Diagnosis of these small Gleason 3-tumours, sometimes consisting of few atypical glands only, strongly depends on the presence cytological features of malignancy, whereas architectural features are less decisive. Even in conventional histology the distinction between reactive changes and malignancy can be very difficult and only be decided by additional immunohistological techniques (2). For diagnosis of these small lesions of well differentiated tumour, examination of FFPE material including subsequent immunohistological examinations were superior to the FCM scans. Our tests show that pre-treatment with alcohol and AO does not

Table 3 Analysis of reasons for false-negative diagnoses

Biopsy	FFPE		FCM (UT)		FCM (BT)		Reason for false-negative diagnosis
	Size	Gleason	Carcinoma	Atyp. glands	Carcinoma	Atyp. glands	
P01–02	0.5	3+3	0	1	0	0	Small groups well differentiated glands
P01–03	0.5	3+3	0	0	0	1	Small groups well differentiated glands
P01–06	1.8	3+3	1	0	1	0	
P01–08	2	3+3	1	0	1	0	
P01–09	8	3+3	1	0	1	0	
P01–12	1	3+3	0	0	0	1	Small groups well differentiated glands
P03–06	3.5	4+3	1	0	1	0	
P03–09	2	3+4	1	0	1	0	
P05–07	4	3+3	1	0	0	1	Misinterpretation as reactive changes
P07–02	3	3+4	1	0	0	1	Insufficient quality of FCM scan
P07–03	3	3+4	1	0	1	0	
P07–04	8.5	3+4	1	0	1	0	
P07–10	7.5	3+3	1	0	1	0	
P07–12	3	3+3	0	1	0	1	Insufficient quality of FCM scan
P09–07	0.5	4+4	1	0	1	0	
P09–08	2	4+4	1	0	1	0	
P09–09	10	4+3	1	0	1	0	
P09–11	2.2	4+4	1	0	1	0	
P09–12	8	4+4	1	0	1	0	

Overview of all 19 tumour-involved biopsies demonstrating tumour-size and Gleason-pattern in conventional histology (FFPE). In FCM ratings included the diagnosis of carcinoma or presence of atypical glands not diagnostic for carcinoma. FFPE, formalin fixed paraffine embedded; FCM, fluorescence confocal microscopy.

induce any restrictions for subsequent FFPE processing and immunohistology, which otherwise would preclude FCM for the assessment of prostate biopsies in our opinion.

Major limitation of the present work is its sample size. As part of an ongoing prospective multi center study, we currently perform further examinations on larger series to explore the chances and limitations of FCM as well as training effects in the detection of small tumour lesions. The expansion of the FCM by a further fluorescence mode (personal communication with the manufacturer) might display the basal cell layer, which can be expected to result in a significant increase of diagnostic reliability.

The immediate feedback provides the surgeon with the opportunity to intra-operatively re-evaluate and modify the biopsy removal strategy in reducing the number of biopsies obtained in case of evidence of malignancy or taking

more biopsies from the regions of interest respectively when there is a discrepancy between high PIRADS and benign or unsuspicious histologic findings. Furthermore, recent findings demonstrate a very good feasibility of FCM for real-time assessment of surgical margins during prostatectomy. The advantages of FCM analysis of peri-prostatic tissue were fast and simple tissue handling and no need for a dedicated set-up; fast acquisition of high-resolution images similar in appearance to H&E stained images and instant availability of images (23).

Recent studies of biopsies from metastatic sites in patients with advanced PCa revealed potentially actionable or prognostic genomic alterations (24,25). Molecular markers will become further important for risk stratification and clinical management of PCa in the future and it will be eligible to preserve tumour involved tissue for molecular
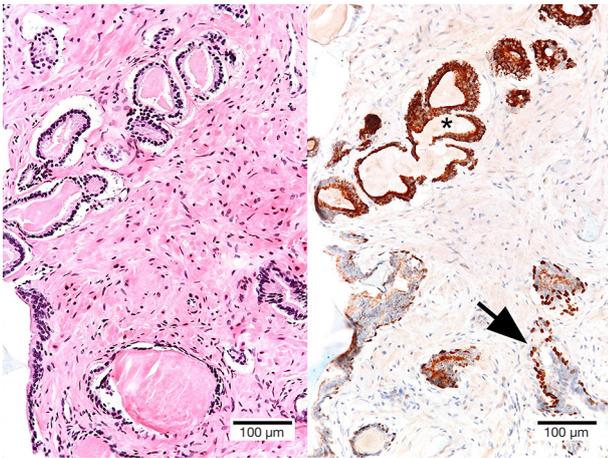
1330

Titze et al. Feasibility of FCM in the assessment of prostate biopsies

Figure 4 Characterisation of small atypical glands in conventional H&E-morphology and additional immuno-histology. H&E-stains (left) show small atypical acinar structures in linear arrangement. Immuno-histology reveals preserved nuclear staining for p40 in the basal cell layer of pre-existing non-neoplastic glands (arrow). Atypical luminal epithelium of tumour glands shows a marked expression of AMACR (*). H&E, haematoxylin-eosin.

Figure 5 FISH for HER2 and CEP17 in material pre-treated for FCM. Despite pre-treatment with AO, fluorescence microscopy shows preserved staining of nuclei with DAPI. ISH signals for HER2 (ZyGreen) and CEP17 (ZyOrange) are clearly separated. There is no interference detectable between AO and ZyGreen. FISH, fluorescence in situ hybridization; FCM, fluorescence confocal microscopy; AO, acridine orange.

analysis. In our additional tests, FCM has proven to be a material sparing method preserving the tissue as lossless native material feasible for subsequent for FISH- and PCR-based analyses. Since AO obtains similar absorption and emission spectra as the fluorochromes frequently used in

routine diagnostics, delicate ZyGreen/FITC-linked signals could be of limited use in subsequent FISH analyses. However, no interference was assumed due to the low penetration depth of AO by incubation for 30 seconds. Subsequent fluorescence-based analyses should therefore be carried out using less superficial areas of the specimen. For the same reason, there is also no limitation to be expected in the amount and quality of extractable DNA.

In recent years advances in the field of prostate MRI and the desire to reduce treatment morbidities have led to a rapid growth in focal treatments for PCa. Each of these modalities is characterized by a significant rate of PCa persistence within treatment zones (6–50%) and the presence of residual cancer within the prostate on re-biopsy (24–49%) (26). Due to its possibility of timely diagnosis of relevant PCa, FCM could provide the opportunity for intraoperative assessment of tumour spread based on mapping biopsies in real-time correlation with MRI-findings. This concept might lead to improved targeting of ablation zones and so could raise the efficacy of focal treatments.

Footnote

References

1. Ferlay J, Soerjomataram I, Dikshit R, Eser S, Mathers C, Rebelo M, Parkin DM, Forman D, Bray F. Cancer incidence and mortality worldwide: sources, methods and major patterns in GLOBOCAN 2012. Int J Cancer 2015;136:E359-86.

2. Magi-Galluzzi C. Prostate cancer: diagnostic criteria and role of immunohistochemistry. Mod Pathol 2018;31:S12-21.

3. Epstein JI, Allsbrook WC Jr, Amin MB, Egevad LL, Committee IG. The 2005 International Society of Urological Pathology (ISUP) Consensus Conference on Gleason Grading of Prostatic Carcinoma. Am J Surg Pathol 2005;29:1228-42.

4. Epstein JI, Egevad L, Amin MB, Delahunt B, Srigley JR, Humphrey PA, Grading C. The 2014 International Society of Urological Pathology (ISUP) Consensus Conference on Gleason Grading of Prostatic Carcinoma: Definition of Grading Patterns and Proposal for a New Grading System. Am J Surg Pathol 2016;40:244-52.

5. Mottet N, Bellmunt J, Bolla M, Briers E, Cumberbatch MG, De Santis M, Fossati N, Gross T, Henry AM, Joniau S, Lam TB, Mason MD, Matveev VB, Moldovan PC, van den Bergh RCN, Van den Broeck T, van der Poel HG, van der Kwast TH, Rouviere O, Schoots IG, Wiegel T, Cornford P. EAU-ESTRO-SIOG Guidelines on Prostate Cancer. Part 1: screening, diagnosis, and local treatment with curative intent. Eur Urol 2017;71:618-29.

6. Klein EA, Cooperberg MR, Magi-Galluzzi C, Simko JP, Falzarano SM, Maddala T, Chan JM, Li J, Cowan JE, Tsiatis AC, Cherbavaz DB, Pelham RJ, Tenggara-Hunter I, Baehner FL, Knezevic D, Febbo PG, Shak S, Kattan MW, Lee M, Carroll PR. A 17-gene assay to predict prostate cancer aggressiveness in the context of Gleason grade heterogeneity, tumor multifocality, and biopsy undersampling. Eur Urol 2014;66:550-60.

7. Kohaar I, Petrovics G, Srivastava S. A rich array of prostate cancer molecular biomarkers: opportunities and challenges. Int J Mol Sci 2019;20:1813.

8. Wilhelm S, Gröbler B, Gluch M, Heinz H. Confocal Laser Scanning Microscopy. Principles. Carl Zeiss GmbH.

9. Agozzino M, Moscarella E, Babino G, Caccavale S, Piccolo V, Argenziano G. The use of in vivo reflectance confocal microscopy for the diagnosis of melanoma. Expert Review of Anticancer Therapy 2019;19:413-21.

10. Hartmann D, Ruini C, Mathemeier L, Bachmann MR, Dietrich A, Ruzicka T, von Braunmuhl T. Identification of ex-vivo confocal laser scanning microscopic features of melanocytic lesions and their histological correlates. J Biophotonics 2017;10:128-42.

11. Ragazzi M, Piana S, Longo C, Castagnetti F, Foroni M, Ferrari G, Gardini G, Pellacani G. Fluorescence confocal microscopy for pathologists. Mod Pathol 2014;27:460-71.

12. Puliatti S, Bertoni L, Pirola GM, Azzoni P, Bevilacqua L, Eissa A, Elsherbiny A, Sighinolfi MC, Chester J, Kaleci S, Rocco B, Micali S, Bagni I, Bonetti LR, Maiorana A, Malvehy J, Longo C, Montironi R, Bianchi G, Pellacani G. Ex vivo fluorescence confocal microscopy: the first application for real-time pathological examination of prostatic tissue. BJU Int 2019;124:469-76.

13. Bertoni L, Puliatti S, Reggiani Bonetti L, Maiorana A, Eissa A, Azzoni P, Bevilacqua L, Spandri V, Kaleci S, Zoeir A, Sighinolfi MC, Micali S, Bianchi G, Pellacani G, Rocco B, Montironi R. Ex vivo fluorescence confocal microscopy: prostatic and periprostatic tissues atlas and evaluation of the learning curve. Virchows Arch 2020;476:511-20.

14. Gareau DS, Li Y, Huang B, Eastman Z, Nehal KS, Rajadhyaksha M. Confocal mosaicing microscopy in Mohs skin excisions: feasibility of rapid surgical pathology. J Biomed Opt 2008;13:054001.

15. MAVIG GmbH. VivaScope® 2500M-G4. Technical Data. 2019.

16. Kasten FH. Cytochemical studies with acridine orange and the influence of dye contaminants in the staining of nucleic acids. Int Rev Cytol 1967;21:141-202.

17. Fleiss J, Cohen J. The equivalence of weighted kappa and the intraclass correlation coefficient as measures of reliability. Educ Psychol Meas 1973;33:613-9.

18. Landis JR, Koch GG. The measurement of observer agreement for categorical data. Biometrics 1977;33:159-74.

19. Ausch C, Buxhofer-Ausch V, Oberkanins C, Holzer B, Minai-Pour M, Jahn S, Dandachi N, Zeillinger R, Kriegshauser G. Sensitive detection of KRAS mutations in archived formalin-fixed paraffin-embedded tissue using mutant-enriched PCR and reverse-hybridization. J Mol Diagn 2009;11:508-13.

20. Glaser AK, Reder NP, Chen Y, Yin C, Wei L, Kang S, Barner LA, Xie W, McCarty EF, Mao C, Halpern AR, Stoltzfus CR, Daniels JS, Gerner MY, Nicovich PR, Vaughan JC, True LD, Liu JTC. Multi-immersion open-top light-sheet microscope for high-throughput imaging of cleared tissues. Nat Commun 2019;10:2781.

21. Wang M, Kimbrell HZ, Sholl AB, Tulman DB, Elfer KN, Schlichenmeyer TC, Lee BR, Lacey M, Brown JQ. High-resolution rapid diagnostic imaging of whole

1332

Titze et al. Feasibility of FCM in the assessment of prostate biopsies

prostate biopsies using video-rate fluorescence structured illumination microscopy. Cancer Res 2015;75:4032-41.

22. Yadav R, Mukherjee S, Hermen M, Tan G, Maxfield FR, Webb WW, Tewari AK. Multiphoton microscopy of prostate and periprostatic neural tissue: a promising imaging technique for improving nerve-sparing prostatectomy. J Endourol 2009;23:861-7.

23. Rocco B, Sighinolfi MC, Bertoni L, Spandri V, Puliatti S, Eissa A, Reggiani Bonetti L, Azzoni P, Sandri M, De Carne C, Turri F, Cimadamore A, Montironi R, Maiorana A, Micali S, Bianchi G, Pellacani G. Real-time assessment of surgical margins during radical prostatectomy: a novel

approach that uses fluorescence confocal microscopy for the evaluation of peri-prostatic soft tissue. BJU Int 2020;125:487-9.

24. Beltran H, Antonarakis ES, Morris MJ, Attard G. Emerging molecular biomarkers in advanced prostate cancer: translation to the clinic. Am Soc Clin Oncol Educ Book 2016;35:131-41.

25. Castro E, Eeles R. The role of BRCA1 and BRCA2 in prostate cancer. Asian J Androl 2012;14:409-14.

26. Ahdoot M, Lebastchi AH, Turkbey B, Wood B, Pinto PA. Contemporary treatments in prostate cancer focal therapy. Curr Opin Oncol 2019;31:200-6.